# Prognostic Health Monitoring of DC Microgrid with Fault Detection and Localization using Machine Learning Techniques

Bharat Bohara, Student Member, IEEE

Electrical and Computer Engineering

University of Houston

Houston, United States

bbohara@uh.edu

Harish S. Krishnamoorthy, Senior Member, IEEE

Electrical and Computer Engineering

University of Houston

Houston, United States
hskrishn@uh.edu

Abstract-DC microgrids incorporate several converters for distributed energy resources connected to different passive or active loads. The complex interactions between the converters and component failures can significantly affect the grids' resilience and real-time health; hence, they must be continually assessed. This paper presents a machine learning-assisted prognostic health monitoring (PHM) and diagnosis approach, enabling progressive interactions between the converters at multiple nodes to dynamically evaluate the grid's (or microgrid's) health status. By measuring the net impedance at the terminals of the power converters at various grid nodes, a neural network-based classifier helps assess the grid's health status and identify the potential faultprone zones, including the fault type and location identification in any arbitrary grid topology. A neural network-based regression model predicts the source power delivered and the loads at different terminals of a healthy grid. Further, Naive Bayes and support vector machine-based classifiers help identify the fault location and type that occurred in a faulty grid. The proposed concepts are supported by detailed analysis and simulation results in a hypothetical four-terminal DC microgrid topology and a standard IEEE 5 Bus system.

Index Terms—Prognostic Health Monitoring, DC Microgrids, Machine Learning, Impedance Measurement

### I. INTRODUCTION

Increased penetration of distributed energy resources (DERs), i.e., the solar, wind, battery, and different passive or active loads, has led to the use of multiple interconnected power conversion units. DC microgrids are sensitive to minor disturbances and faults due to their lower inertia and converters' nonlinear switching behaviors. The disturbances can happen due to distributed source power variations, load fluctuations, temporary faults occurrences, and communication channel failures or delays [1]. Moreover, an erratic topological modification due to irregular power generation scenarios and dynamic loads contributes to higher grid instability and fault incidents. Therefore, detecting the load characteristics (upon increased or decreased loads) and the state of the DERs (during abrupt addition or removal, either due to faults or power generation shut-down) can enable an immediate diagnosis or improvement in the overall system resiliency. In this paper, a robust analytical strategy is developed to improve the resiliency in microgrids via impedance measurement techniques observed from a particular converter side, which is a computationally efficient and cheaper method. The impedance of an arbitrary system has a lot of interesting characteristics that can be used to unlock hidden patterns within the system's performance and dynamics. Two critical factors affecting the grid resiliency are fast fault detection and localization, considering that even a momentary surge current flow can damage the power converters and delicate loads during a fault occurrence.

Examining the load impedance is of utmost importance as it reveals the converter's overall stability, as assessed by the Middlebrook criteria. Various approaches have been suggested in the literature to assess the stability of DC microgrids in real-time, employing impedance-based analysis. The presence of nonlinear switching power converters in DC microgrids adds complexity to the system dynamics [2]. One standard method to evaluate large-signal linearized stability is by studying small-signal linearized stability, as discussed in [3]. Researchers have introduced two methods for small signal-based impedance measurement: narrowband using sine waves and wideband using white noise injection signals. The wideband approach is more efficient due to its capability of implementing Fast Fourier Transformation (FFT) on a digital controller, which outperforms the narrowband system requiring specialized instruments for measurement. Furthermore, researchers have conducted online power impedance identification using Hardware-in-the-Loop (HiL) tools in [4].

A small perturbation signal is injected through a specific converter over a wide frequency range to determine the impedance and phase-shift characteristics. Papers [5], [6] proposed an empirical mode decomposition (EMD)-based CNN classifier which uses fault current characteristics to detect and classify normal, faulty, and abnormal (over-voltage, overload, and light load) conditions under different fault resistances, locations, and various system conditions. The power converters exhibit nonlinear dynamics because of the switching instances, adding additional complexity to an intricately growing DC microgrid. This further leads to a lack of grid inertia, making the DC microgrid prone to significant instability upon sudden changes in any distributed sources or the inter-connected

loads. Embedded impedance-based protection techniques have i) lower noise due to the absence of communication channels, ii) lower computational cost in monitoring the grid health state, iii) cheap and reduced size of the measurement tools. Unregulated and default operations may lead to costly repairs, time-consuming fault detection and diagnosis processes, hazardous events, damage of expensive and delicate equipment, or even stoppage of the entire system.

Paper [7] proposed a real-time embedded impedance measurement technique based on a Lock-In Amplifier (LIA) by using a minimal perturbation of known frequencies to measure an equivalent incremental impedance of the network and improve overall system stability. Paper [8] extended the work with a Lock-In Amplifier-based fault location technique that uses an advanced digital algorithm to locate the faults accurately. Recent studies have examined and enhanced the stability of the power grid under uncertain conditions using machine learning tools [9]-[11]. Paper [12] used ANN-based methods to detect the fault types and locations using the transient voltage and current information. The paper [13] presents a machine learning-based method of assessing the online grid health index by continuously measuring impedance at the converter output over a wide range of frequencies, which is perturbed by injecting a sinusoidal PWM signal.

This paper introduces an online method for evaluating grid health, which relies on specific impedance measurements at the converter output, including magnitude and phase over a wide range of frequencies. The proposed approach does not require identifying or grouping sources and loads, thus making it suitable for any dynamically changing systems. The analysis is performed at the output terminals of individual converters, making it an excellent choice for continuously assessing the system's health at any given moment. Moreover, the method offers valuable indicators for effectively reallocating unhealthy zones, along with fault location and type identification within the grid, all without significant additional cost or complexity to the system.

## II. PROPOSED IMPEDANCE-BASED PHM

An impedance observed from the converter of interest (here, observer source as shown in Fig. 7) is measured by injecting an excitation signal (sine wave) at different frequency levels through the converter's gating signal. Consequently, the system response is continuously measured as a function of frequency and, thus, processed to compute the impedance of an unknown grid network located on the other side of the observing converter. Altogether there are three primary stages in the proposed technique to identify the health status of a DC microgrid, as shown in Fig. 1. In stage-1, a trilayered neural network-based classifier (with 100% validation accuracy) is trained to detect whether the grid is healthy or faulty. In stage-2, two different ML models (i.e., regressor and Naive Bayes classifier) are set to run simultaneously. If the grid is healthy, the unknown grid impedance is fed into a neural networkbased regressor (with 99.01% validation accuracy) which predicts its operating conditions, i.e., the power delivered by

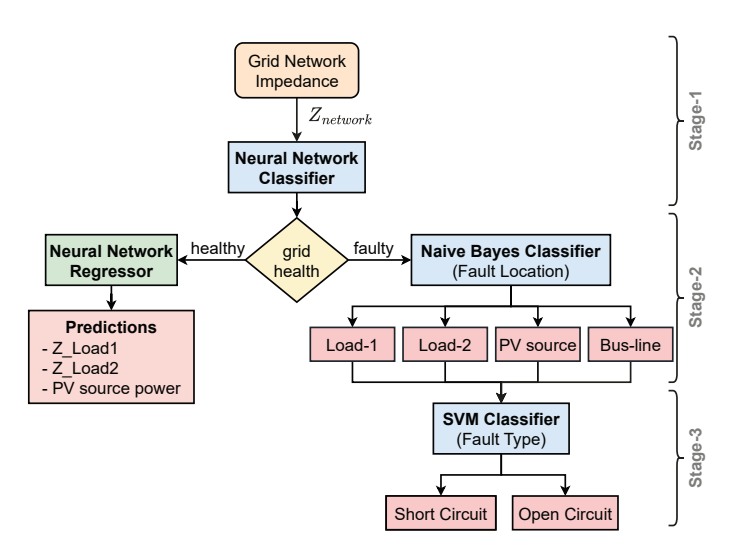


Fig. 1: A proposed method to identify the overall health status of an unknown grid network looking from a particular converter side. The flowchart illustrates the techniques for predicting the operating conditions of a grid network and identifying the fault location and type over the infected area if it existed.

the individual sources and the loading conditions at different nodes of the grid.

On the contrary, if the grid is faulty, the fault location is first identified through a Naive Bayes classifier (with 60.1% validation accuracy). In a four-terminal DC microgrid topology considered in this study, there are altogether four probable faulty sections: the output terminal of the PV source, input ports of Load1 and Load2, and the bus line. Once the faulty section is spotted, in stage-3, an SVM classifier (with 87.9% validation accuracy) is trained to recognize whether the fault is either short-circuit or open-circuit. The grid health and the fault conditions were trained with different ML algorithms. However, the models with the highest test and validation accuracy were selected eventually, i.e., a neural network for predicting the operating conditions of a healthy network, whereas Naive Bayes and SVM classifiers to locate the unhealthy section and detect the fault type if it exists.

An averaged small signal model technique is used to compute the grid network impedance and validate the proposed approach. First, to measure the output impedance of a PV side converter, the state-space equations of a non-ideal boost converter during switch-on and switch-off modes are obtained, as shown in equations (1), and (3), respectively. The output voltage of a boost converter, as seen from the bus terminal, is derived as shown in (5). The PV converter's output impedance is obtained by taking  $\hat{d}(s)$  and  $\hat{v}(s)$  zero, as shown in (6). Finally, as seen from the observer source, the net impedance of the entire grid network is computed via simple circuit theory as depicted in (7).

$$\begin{bmatrix} \dot{i}_L \\ \dot{v}_c \end{bmatrix} = \underbrace{\begin{bmatrix} -\frac{r_L}{L} & 0 \\ 0 & 0 \end{bmatrix}}_{\mathbf{A_1}} \begin{bmatrix} i_L \\ v_c \end{bmatrix} + \underbrace{\begin{bmatrix} 0 & \frac{1}{L} \\ -\frac{1}{C} & 0 \end{bmatrix}}_{\mathbf{B_1}} \begin{bmatrix} i_o \\ v_s \end{bmatrix}$$
(1)

$$\begin{bmatrix} v_o \end{bmatrix} = \underbrace{\begin{bmatrix} 0 & 1 \end{bmatrix}}_{\mathbf{C}_1} \begin{bmatrix} i_L \\ v_c \end{bmatrix} + \underbrace{\begin{bmatrix} -r_c & 0 \end{bmatrix}}_{\mathbf{E}_1} \begin{bmatrix} i_o \\ v_s \end{bmatrix}$$
 (2)

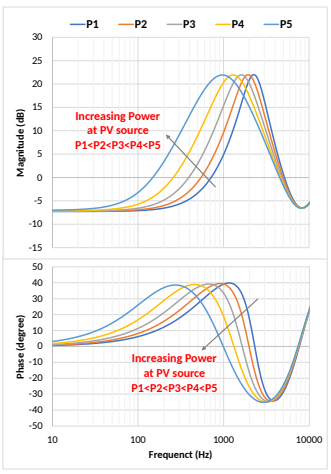


Fig. 2:  $Z_{network}$  distribution under varying PV power

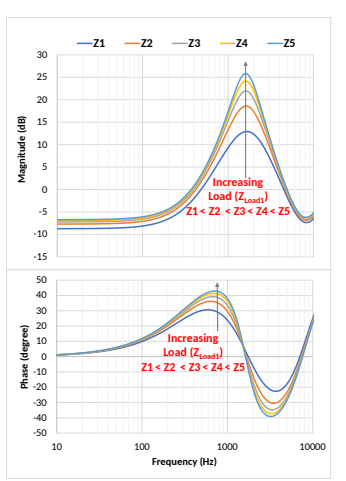


Fig. 3:  $Z_{network}$  distribution under varying load (RL) at Load1

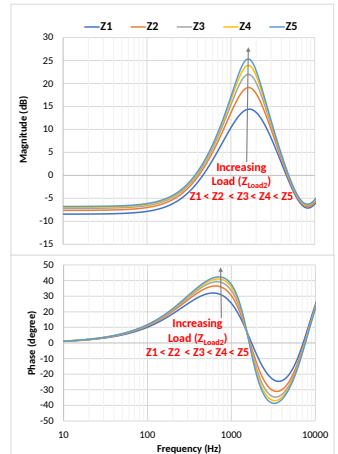


Fig. 4:  $Z_{network}$  distribution under varying load (RL) at Load2

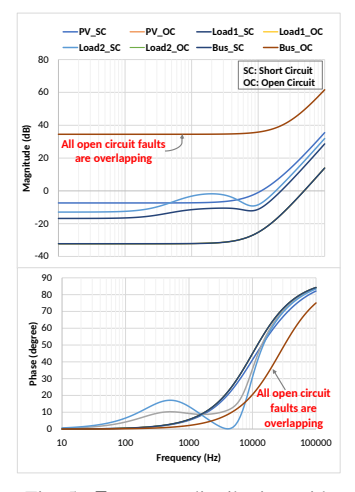


Fig. 5:  $Z_{network}$  distribution with different grid faults and location

$$\begin{bmatrix} \dot{i}_L \\ \dot{v}_c \end{bmatrix} = \underbrace{\begin{bmatrix} -\frac{r_L + r_C}{L} & -\frac{1}{L} \\ \frac{1}{C} & 0 \end{bmatrix}}_{\mathbf{A_2}} \begin{bmatrix} i_L \\ v_c \end{bmatrix} + \underbrace{\begin{bmatrix} \frac{r_c}{L} & \frac{1}{L} \\ -\frac{1}{C} & 0 \end{bmatrix}}_{\mathbf{B_2}} \begin{bmatrix} i_o \\ v_s \end{bmatrix}, \tag{3}$$

$$\begin{bmatrix} v_o \end{bmatrix} = \underbrace{\begin{bmatrix} r_c & 1 \end{bmatrix}}_{\mathbf{C_2}} \begin{bmatrix} i_L \\ v_c \end{bmatrix} + \underbrace{\begin{bmatrix} -r_c & 0 \end{bmatrix}}_{\mathbf{E_2}} \begin{bmatrix} i_o \\ v_s \end{bmatrix}$$
(4)

$$\hat{v}_{o}(s) = \left[ C(sI - A)^{-1} \left( [A_{1} - A_{2}] \begin{bmatrix} i_{L} \\ v_{c} \end{bmatrix} + B_{1}i_{o} + B_{2}v_{s} \right) + [C_{1} - C_{2}] \begin{bmatrix} i_{L} \\ v_{c} \end{bmatrix} + [E_{1} - E_{2}]i_{o}\hat{d}(s) + [C(sI - A)^{-1}B_{1} + E]\hat{i}_{o}(s) + C(SI - A)^{-1}B_{2}\hat{v}_{s}$$
(5)

$$z_{PV} = \frac{\hat{v_o}}{\hat{i_o}} = \frac{(sr_c + \frac{1}{C})(s + \frac{r_L}{L} + \frac{r_c D(1 - D)}{L})}{s^2 + \frac{1}{L}(r_c + r_L - r_c D)s + \frac{1}{LC}(1 - D)^2}$$
 (6)

$$Z_{network} = 2z_{L1} + z_a // z_b // z_c \tag{7}$$

The parameters used in eqn. 1 - 6 are described in table I, and the matrices parameters are defined as below:

$$A = A_1D + A_2(1 - D)$$

$$B = B_1D + B_2(1 - D)$$

$$C = C_1D + C_2(1 - D)$$

$$E = E_1D + E_2(1 - D)$$

$$z_a = 2z_{L2} + z_{Load1}$$

$$z_b = 2z_{L3} + z_{PV}$$

$$z_c = 2z_{L4} + z_{Load2}$$

The datasets used to train the models for identifying the health index of an entire DC microgrid topology, as shown in Fig. 7 is created by varying the power at the PV source and the loading conditions at  $Load_1$  and  $Load_2$  terminals.

TABLE I: PV-side boost converter parameters and variables

Parameters	Description	Units	Parameters	Description	Units
i_L	Inductor current	A	С	Converter capacitance	$\mu F$
r_L	Inductor ESR	Ω	v_s	Source voltage	V
v_c	Capacitor voltage	V	v_o	Output voltage	V
r_c	Capacitor ESR	Ω	i_o	Output current	A
L	Converter inductance	$\mu H$		-	

It can be observed in Fig. 2, 3, and 4, distinct patterns are observed in the grid network impedance as seen from the observer source upon varying PV power and at different loads at  $Load_1$  and  $Load_2$ . Likewise, the grid impedance exhibits clear distinctions under various fault conditions, encompassing both short and open circuit faults, as depicted in Fig. 5, compared to normal operating conditions. The dataset used in this paper comprises 125 healthy cases and 1000 faulty cases. For model training and evaluation, 75% of the entire pool of data points are utilized, while the remaining 25% is reserved as the test set. The healthy and faulty data points show a slight imbalance in quantity; however, this will be addressed in future work through data augmentation techniques. The complete dataset generated to train the regression and classification models can be accessed via https://github.com/Varat7v2/PHM-DC-Microgrid.

# III. RESULTS

Two distinct test scenarios are considered: 1) a simplified grid network topology featuring loads and sources at different nodes, as depicted in Fig. 7, and 2) a standard IEEE 5 bus system, as portrayed in Fig. 12. The performance of the regression and classification models is assessed under different operating conditions in both scenarios.

### A. Case 1: A Simplified 4-terminal DC microgrid topology

First, a neural network-based classifier accurately determines the grid network's health status (healthy or faulty) with 100% accuracy under all test conditions, as detailed in table III. The classifier's performance is visualized using a confusion matrix in Fig. 6(a). In the second stage, if the grid is identified

TABLE II: Neural network-based regressor predictions for a healthy grid network at different operating conditions

$Z_{network}$ at different	PV Power (kW)		$R_{Load1} \atop (\Omega)$		$L_{Load1} \ (\mu H)$		$R_{Load2} \atop (\Omega)$		$L_{Load2} \ (\mu H)$		RMSE
operating conditions	Actual	Prediction	Actual	Prediction	Actual	Prediction	Actual	Prediction	Actual	Prediction	
Normal operation	10	9.9	5.5	5.53	100.5	101.24	5.5	5.5	100.5	100.55	0.3745
PV power increased by 20%	12	11.68	5.5	5.56	100.5	101.86	5.5	4.9	100.5	87.28	6.6536
PV power decreased by 20%	8	7.79	5.5	5.46	100.5	99.55	5.5	5.42	100.5	98.66	1.0417
Load1 increased by 20%	10	9.87	10	9.74	200	194.24	5.5	5.62	100.5	103.18	3.1804
Load1 decreased by 20%	10	9.66	1	0.99	1	0.81	5.5	5.21	100.5	94.11	3.2042
Load2 increased by 20%	10	10.26	5.5	5.36	100.5	97.3	10	10.26	200	205.74	3.2917
Load2 decreased by 20%	10	10.58	5.5	5.46	100.5	99.61	1	0.93	1	-0.44	0.8956

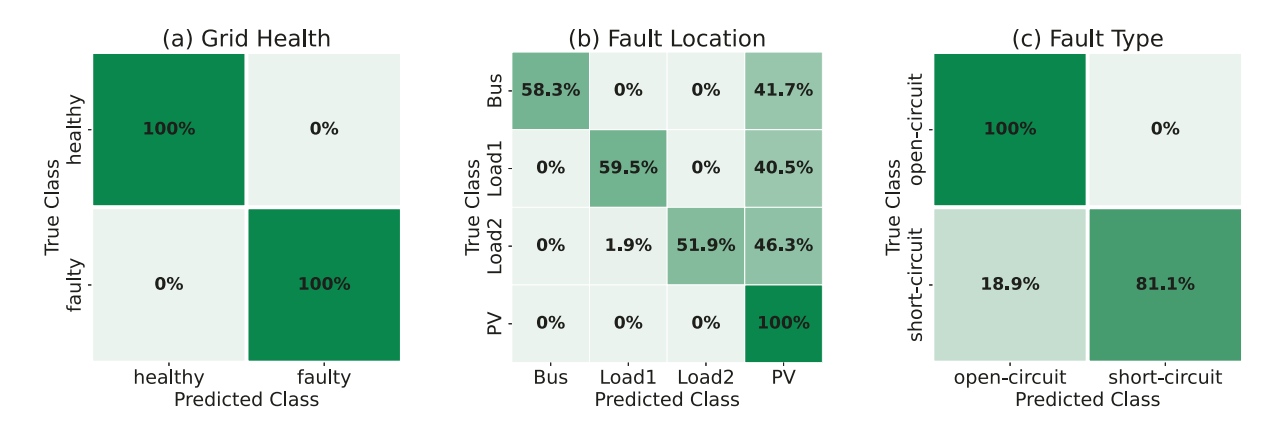


Fig. 6: Confusion matrix of a) Neural Network-based classifier, b) Naive Bayes classifier, and c) SVM classifier evaluated on test dataset

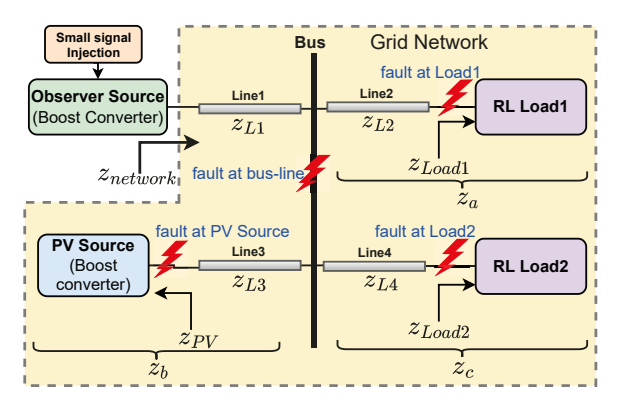


Fig. 7: A four-terminal DC microgrid topology

as healthy, another neural network-based regressor is employed to validate the performance under various operating conditions, including variations in PV power source and load conditions at Load1 and Load2. The regressor consistently achieves an accuracy of 98.55% on the test dataset, and the evaluation results are presented in table II. The regressor performs pretty well, as evidenced by the root mean square error (RMSE) for different test conditions, although the prediction error is slightly higher for increased PV source power. This problem will be thoroughly investigated in future work.

On the other hand, when a grid network is found to be faulty, a Naive Bayes classifier is employed to determine the faulty section in the DC microgrid topology. The classifier achieves a satisfactory fault location accuracy of 69.5%, as illustrated in table III, and the confusion matrix in Fig. 6(b). The model misclassifies 41.7% of bus line faults, 40.5% of

TABLE III: Model performance metrics of different classifiers

Classifiers	Average m	etrics on	test dataset	Model Acc	AUC	
	Precision	Recall	F1-Score	Validation	Test	(%)
	(%)	(%)	(%)	(%)	(%)	
Neural Network	100	100	100	100	100	100
Naive Bayes	86.52	67.41	75.78	61.3	69.5	74
SVM	82.45	100	90.38	86.9	90	88

Load1 side faults, and 46.3% of Load2 side faults, inaccurately identifying them to be located at the PV side. This unavoidable misclassification is due to the lack of distinguishable patterns in the open-circuit faults across all locations, as evident in Fig. 5. Once the fault location is identified, a support vector machine (SVM)-based classifier is employed to recognize the fault type in the affected area, achieving a test accuracy of 90%. The confusion matrix in Fig. 6(c) indicates that 18.9% of the short-circuit faults are misclassified, while all the open-circuit faults are correctly identified.

### B. Case 2: IEEE 5 Bus System

To assess the performance of the proposed technique in a more real-world scenario, a standard IEEE 5 bus system [14] is taken into account. The standard bus architecture provided by IEEE is shown in Fig. 12, and the line data as proposed for a 100 kV and 100 MVA system is presented in table IV. To adapt the line impedances and admittances to a low voltage DC (LVDC) system (400 V and 10 kW) commonly found in data centers and DC grid distribution [15], the p.u. values are scaled down using equations 8 to 10. In this setup, the net effective impedance seen from Bus 1 towards the dense network is computed by injecting a small signal through the converter's gating at Bus 1. The cumulative responses of the

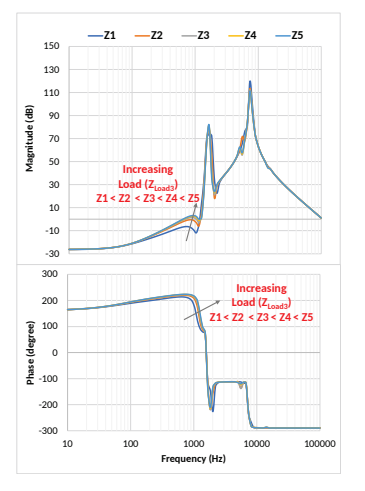


Fig. 8: Impedance plots under varying load at Bus 2

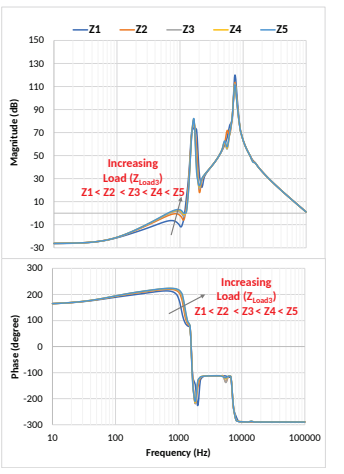


Fig. 9: Impedance plots under varying load at Bus 3

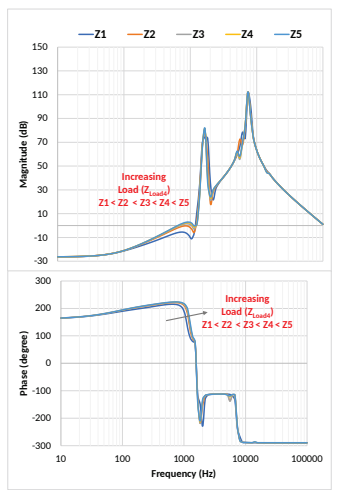


Fig. 10: Impedance plots under varying load at Bus 4

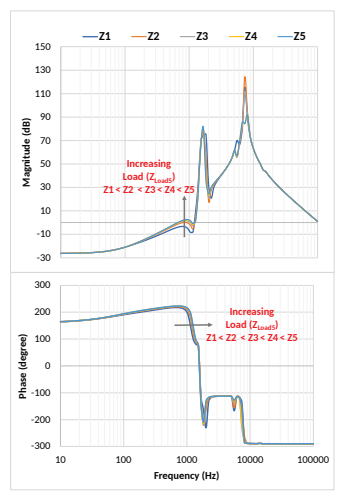


Fig. 11: Impedance plots under varying load at Bus 5

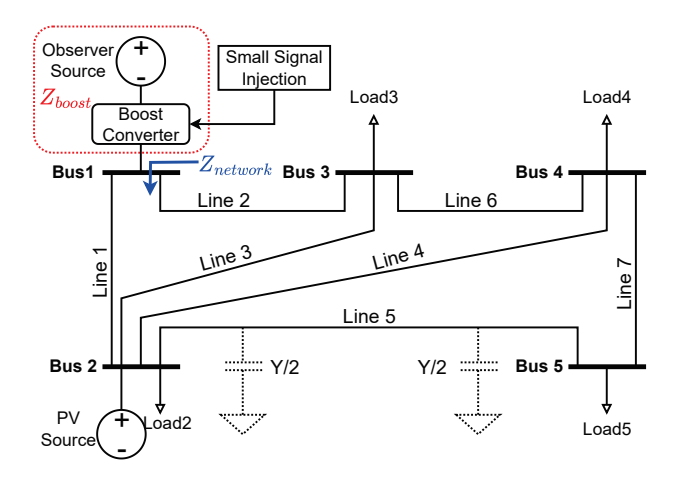


Fig. 12: A standard IEEE 5 bus system architecture

other buses, loads, and sources connected to them are then captured from Bus 1 using the system's admittance matrix, as depicted in eqn. 11 - 13.

TABLE IV: Line data of standard IEEE 5 bus system (100 kV & 100 MVA base), and scaled-down parameters for the proposed system (400 V & 10 kW system)

From Bus	To Bus	Line Impedance R+jX (p.u)	Line Charging Y/2 (p.u)	Scaled down parameters for 400 V, 10 kW system R $(\Omega)$   L $(mH)$   C $(\mu F)$		
1	2	0.02+j0.06	j0.030	0.32	2.5465	4.9736
1	3	0.08+j0.24	j0.025	1.28	10.1859	4.1447
2	3	0.06+j0.18	j0.020	0.96	7.6394	3.3157
2	4	0.06+j0.18	j0.020	0.96	7.6394	3.3157
2	5	0.04+j0.12	j0.015	0.64	5.0930	2.4868
3	4	0.01+j0.03	j0.010	0.16	1.2732	1.6579
4	5	0.08+j0.24	j0.025	1.28	10.1859	4.1447

$$R_{scaled} = R_{p.u} \cdot \frac{kV_{base}^2}{MVA_{base}} \tag{8}$$

$$L_{scaled} = \frac{X_{p.u} \cdot \frac{kV_{base}^2}{MVA_{base}}}{\omega} \tag{9}$$

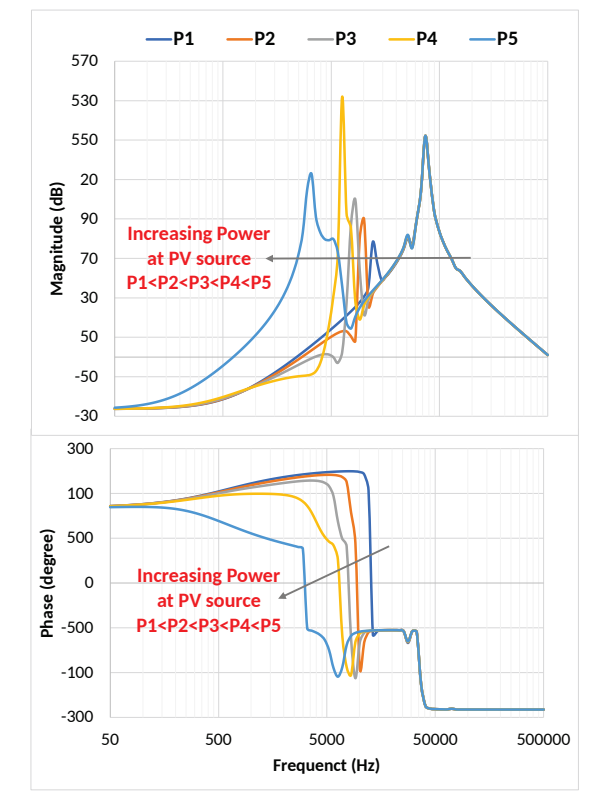


Fig. 13: Impedance plots under varying PV source power at Bus 2

$$C_{scaled} = \frac{(Y/2)_{p.u}}{\omega \cdot \frac{kV_{base}^2}{MVA_{base}}}$$
(10)

where,  $\omega=2\pi f$ , and f=60Hz is the grid frequency.  $R_{scaled}$ ,  $L_{scaled}$ , and  $C_{scaled}$  represent the actual resistance, inductance, and capacitance of the considered system, which operates at 400V and 10kW. On the other hand,  $R_{p.u}$ ,  $X_{p.u}$ , and  $Y/2_{p.u}$  denote the line impedance and charging in per unit (p.u.) values for a standard IEEE 5 Bus system with a voltage

of 100kV and a capacity of 100MVA, as shown in table IV. To adapt to the scaled-down system, the base voltage is set to be  $(kV_{base})$  as 400V, and considering the DC nature of the system, the reactive power is zero, making the apparent power equal to the active power (i.e., S (kVA) = P (kW)). Thus, the base apparent power  $(MVA_{base})$  is 10kW.

$$Y_{bus} = \begin{bmatrix} Y_{11} & -y_{12} & -y_{13} & -y_{14} \\ -y_{12} & Y_{22} & -y_{23} & -y_{24} \\ -y_{13} & -y_{23} & Y_{33} & -y_{34} \\ -y_{14} & -y_{24} & -y_{34} & Y_{44} \end{bmatrix}$$
(11)

$$Z_{bus} = Y_{bus}^{-1} \tag{12}$$

$$Z_{network} = Z_{bus(1,1)} - Z_{boost}$$
 (13)

where,  $Y_{bus}$  and  $Z_{bus}$  are the admittance and impedance matrix of the overall system,  $Z_{network}$  is the network impedance observed from Bus 1,  $Z_{bus(1,1)}$  is the net effective impedance at Bus 1 looking from the top and  $Z_{boost}$  is self-impedance of Bus1.

As shown in Fig. 8-11, a slight change is observed in the impedance magnitude and phase plots under varying loading conditions on buses 2, 3, 4, and 5. Enhancement of these patterns can be achieved by selecting an appropriate operating condition range, a subject that will be further explored in future research. In contrast, distinguishable patterns are apparently observed in magnitude and phase plots under varying PV source power as depicted in Fig. 13. This indicates that by examining impedance plots from a specific bus in a densely interconnected bus system, it becomes possible to predict the overall grid health condition and detect changes in loads and sources at other parts of the unknown grid network.

### IV. CONCLUSION

This paper introduces a prognostic health monitoring and diagnosis strategy for DC microgrids based on impedance measurements. The approach involves injecting sinusoidal perturbations of PWM signals into one or more interconnected converters within the grid and then measuring the corresponding impedance at the converter's output terminals. Considering the advancement and potential of different machine learning techniques, impedance-based feature learning techniques were incorporated with machine learning to predict the unknown grid topology health conditions. The results show that grid network impedance measured at the converter terminals has unique patterns for each operating condition, which is further used to classify the overall health status of the grid, achieving a classification accuracy of 100% using neural network architecture. Further, the same impedance-based features are used to locate (with an accuracy of 69.5% using the Naive Bayes classifier) and identify the fault type (with an accuracy of 86.9% using the SVM classifier) in the unhealthy grid zones. The proposed grid health prognosis and monitoring scheme enables continual health gauging of an intricate grid network, where prior control actions can be taken into account to maintain future grid resiliency under adverse conditions. The results are verified on a simple four-terminal grid network topology and a standard IEEE 5 Bus system. In future work, the proposed technique will be implemented on a complex grid network topology consisting of energy storage and closed-loop control systems.

### ACKNOWLEDGMENT

This material is partly based upon work supported by the National Science Foundation under Grant No. 2239966.

### REFERENCES

- S. T. Ojetola, M. J. Reno, J. Flicker, D. Bauer, and D. Stoltzfuz, "Testing machine learned fault detection and classification on a dc microgrid," 2022 IEEE Power and Energy Society Innovative Smart Grid Technologies Conference, ISGT 2022, 2022.
- [2] R. K. Gaddala, M. G. Majumder, and K. Rajashekara, "Dc-link voltage stability analysis of grid-tied converters using dc impedance models," *Energies 2022, Vol. 15, Page 6247*, vol. 15, p. 6247, 8 2022. [Online]. Available: https://www.mdpi.com/1996-1073/15/17/6247
- [3] R. A. Jacob, S. Member, S. Senemmar, J. Zhang, and S. Member, "Fault diagnostics in shipboard power systems using graph neural networks."
- [4] N. Mohammed, M. Ciobotaru, and G. Town, "Performance evaluation of wideband binary identification of grid impedance using grid-connected inverters," 2019 21st European Conference on Power Electronics and Applications, EPE 2019 ECCE Europe, 9 2019.
- [5] D. Patil and S. Thale, "Deep neural network enabled fault detection in lvdc microgrid using empirical mode decomposition," *International Journal of Advanced Technology and Engineering Exploration*, vol. 9, pp. 2394–7454. [Online]. Available: http://dx.doi.org/10.19101/IJATEE.2021.874973
- [6] D. D. Patil and S. Thale, "A novel method for real time protection of dc microgrid using cumulative summation and wavelet transform 311 original scientific paper."
- [7] F. Paz and M. Ordonez, "An embedded impedance measurement for dc microgrids based on a lock-in amplifier," 2016 IEEE 7th International Symposium on Power Electronics for Distributed Generation Systems, PEDG 2016, 7 2016.
- [8] —, "Embedded fault location in dc microgrid systems based on a lock-in amplifier," 2017 IEEE 8th International Symposium on Power Electronics for Distributed Generation Systems, PEDG 2017, 7 2017.
- [9] G. Roeder, L. Ott, A. Meier, B. Wunder, P. Wienzek, A. Baermann, F. Liers, and M. Schellenberger, "Analysis and improvement of lvdc-grid stability using circuit simulation and machine learning-a case study," in NEIS 2021; Conference on Sustainable Energy Supply and Energy Storage Systems. VDE, 2021, pp. 1–7.
- [10] A. Sepehr, O. Gomis-Bellmunt, and E. Pouresmaeil, "Employing machine learning for enhancing transient stability of power synchronization control during fault conditions in weak grids," *IEEE Transactions on Smart Grid*, vol. 13, pp. 2121–2131, 5 2022.
- [11] B. Hangun, O. Eyecioglu, and M. Beken, "Forecasting the stability of a 4-node architecture smart grid using machine learning," 10th International Conference on Smart Grid, icSmartGrid 2022, pp. 440– 442, 2022
- [12] N. K. Chanda and Y. Fu, "Ann-based fault classification and location in mvdc shipboard power systems," NAPS 2011 - 43rd North American Power Symposium, 2011.
- [13] H. Sayed, B. Bohara, and H. S. Krishnamoorthy, "Embedded Impedance Measurement for DC Microgrid Towards PHM and Control," in 2022 IEEE International Conference on Power Electronics, Drives and Energy Systems (PEDES), Dec. 2022, pp. 1–6.
- [14] B. S, A. S, V. S. C, J. R, and S. H. V, "Big Data from Actual IEEE 5 Bus System during Normal and Control Operations," Nov. 2022. [Online]. Available: https://ieee-dataport.org/documents/ big-data-actual-ieee-5-bus-system-during-normal-and-control-operations
- [15] L. Li, K.-J. Li, K. Sun, Z. Liu, and W.-J. Lee, "A comparative study on voltage level standard for dc residential power systems," *IEEE Transactions on Industry Applications*, vol. 58, no. 2, pp. 1446–1455, 2022.